Microbial siderophore production is tightly coupled to iron in hydrothermal plumes

Colleen L. Hoffman[1,2,3*], Patrick J. Monreal[3,4], Justine B. Albers[5], Alastair J.M. Lough[6], Alyson E. Santoro[5], Travis Mellett[3,7], Kristen N. Buck[7], Alessandro Tagliabue[8], Maeve C. Lohan[6], Joseph A. Resing[1,2,3], Randelle M. Bundy[3*]

1- Joint Institute for the Study of Atmosphere and Ocean, University of Washington, 3737 Brooklyn Avenue NE, Seattle, WA 98195, USA

2-Cooperative Institute for Climate, Ocean, and Ecosystem Studies, University of Washington, 3737 Brooklyn Avenue NE, Seattle, WA 98195, USA

3-School of Oceanography, University of Washington, 1501 NE Boat Street, Seattle, WA 98195, USA

4- Department of Earth System Science, Stanford University, 473 Via Ortega, Stanford, CA 94305, USA

5- Department of Ecology, Evolution, and Marine Biology, University of California, Santa Barbara, CA 93106, USA

6-Department of Ocean and Earth Sciences, National Oceanography Centre, University of Southampton, European Way, Southampton SO14 3ZH, United Kingdom

7- College of Marine Science, University of South Florida, 140 7th Avenue South, St. Petersburg, FL, 33701, USA

8-Department of Earth, Ocean, and Ecological Sciences, University of Liverpool, 4 Brownlow Street, Liverpool l69 3GP, United Kingdom

*Corresponding authors clhoffma@uw.edu, rbundy@uw.edu

Abstract

Specialized molecules, such as siderophores, are used to access and retain iron in soluble forms by marine microorganisms. These siderophores form part of the ocean dissolved iron-binding ligand pool and are hypothesized to exert a key control on the persistence of iron in hydrothermal environments. To explore this hypothesis, we measured iron, iron-binding ligands, and siderophores from 11 geochemically distinct sites along a 1,700 km section of the Mid-Atlantic Ridge. We found siderophores at all sites and proximity to the vent played an important role in dictating siderophore types and diversity. The notable presence of amphiphilic siderophores may enable microbes to access particulate iron in hydrothermal plumes. The tight coupling between strong ligands and dissolved iron across six distinct hydrothermal environments, combined with the local presence of siderophore producing microbial genera suggests that biological production of siderophores exerts a key control on hydrothermal dissolved iron concentrations.

Introduction

Over the last few decades, observations and modelling efforts have increased our understanding about the critical role organic ligands play in the cycling, transport, and utilization of trace metals[1–4]. Strong iron-binding organic ligands (L_1), such as siderophores, are thermodynamically favored to complex and stabilize external sources of iron (Fe) and prevent its scavenging and removal. This is particularly important when ligands are present in excess of dissolved Fe (dFe)[5]. For example, in high dissolved and particulate Fe estuarine systems, only the dFe that escapes estuarine flocculation is bound to the strongest Fe-binding ligands[6,7].

Siderophores are a type of strong ligand produced by bacteria and fungi to facilitate uptake of Fe by complexation of Fe in the high affinity siderophore, drawing Fe out of otherwise inaccessible phases in the marine environment[8,9]. Historically, due to the energy required to produce siderophores, they have only primarily been considered as an important microbial strategy for Fe acquisition in the low-Fe surface ocean[8,10]. Compared to terrestrial soil ecosystems – where siderophores were first identified – Fe is several orders of magnitude lower in the marine environment. Their production could be a widespread microbial Fe acquisition strategy, which then tightly controls the utilization and availability of Fe[11]. A recent study identified siderophores in oxygen-deficient zones with relatively high Fe concentrations (>2 nM),

suggesting they are important for both Fe acquisition and offshore transport of Fe away from sediment sources[2,4,6,12,13]. Genetic evidence in the Guaymas Basin hydrothermal system also showed that >70% of Fe-related bacterial transcripts were involved in siderophore uptake, regulation, and biosynthesis, providing additional evidence that siderophore production and uptake may be important even in the higher Fe environments of the deep ocean[14].

While siderophore production could be common in the deep ocean[3], none of the previous studies have directly measured siderophores in hydrothermal systems, explored the mechanisms for their production, or determined their impact on Fe cycling in the ocean interior. This represents an important gap in our understanding of how hydrothermal sources may regulate the deep ocean dFe inventory. Here, for the first time, we identified the presence of siderophores and siderophore producing microbes in 11 geochemically distinct hydrothermal environments, including four black smokers (high temperature, high Fe), four sites off-axis sites (within 30 km of black smokers), one diffuse-flow vent (low temperature, low Fe), one alkaline vent (pH 9-11, very low Fe), and one non-vent fracture zone along the slow-spreading (20-50 mm/yr) Mid-Atlantic Ridge (MAR) to understand whether microbial ligand production impacts the supply of hydrothermal dFe to the ocean. Overall, our results show microbially-produced siderophores were present in all sites and that strong L_1 ligands including siderophores exert a tight control on hydrothermal dFe. This suggests that strong organic ligands produced by bacteria play a key role in setting deep ocean Fe concentrations across global hydrothermal systems.

Results and Discussion

L_1 iron-binding ligands and the role of siderophores in hydrothermal plumes

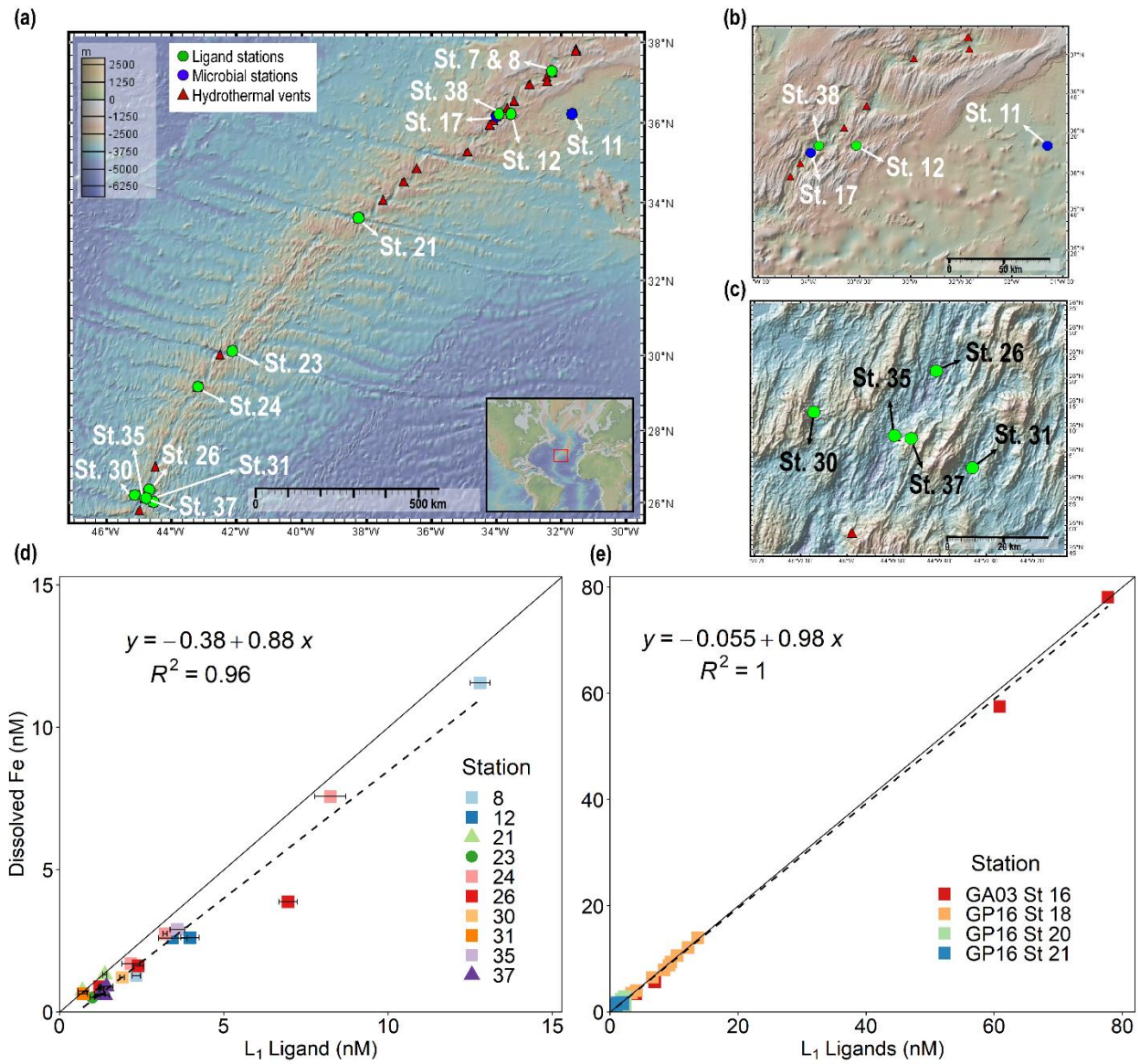

Figure 1. Dissolved iron is strongly correlated with L_1 iron-binding ligands in diverse hydrothermal systems. (a) Station map showing the 11 sites investigated along the MAR. Known hydrothermal vents are marked as red triangles[15]. Two expanded inset maps for (b) Rainbow and (c) TAG hydrothermal vent fields. For additional information about vent site characteristics refer to **Table 1**. (d) dFe versus L_1 iron-binding ligands at each vent site in this study showing a ~1:1 correlation (m= 0.88, R^2 = 0.96) with dFe in neutrally-buoyant plumes along the MAR. (e) dFe versus L_1 ligands from previous studies over the ridge axis and ~80 km from ridge axis in the Southern East Pacific Rise hydrothermal plume[2], and over TAG hydrothermal vent field[12]. The solid black lines in (d) and (e) are the 1:1 ratio line between dFe and ligand concentrations, and dashed lines show the linear regression for the corresponding data. Square symbols refer to spreading centers, triangles refer to fracture zones, and circles refer to alkaline vents. Error bars represent the 95% confidence interval of the data fit as calculated by ProMCC[16]. The map was created using GeoMapApp version 3.6.14.

The L_1 Fe-binding organic ligand pool is a heterogeneous mixture of compounds that are operationally classified based on their binding strength with Fe (log $K^{cond}_{Fe',FeL}$ > 12). These L_1

ligands have been proposed to be important for stabilizing and transporting Fe in hydrothermal plumes[1,2,17]. Here, the average binding strength (log $K^{cond}_{Fe',FeL}$) and concentration of organic Fe-binding ligands were quantified in multiple vent systems that spanned a wide range in dFe concentrations (0.41-90.3 nM). Over >99% of the dFe was complexed by L_1 ligands, which meant Fe-free L_1 ligands capable of binding additional Fe were generally present in low concentrations (< 1 nM; **Fig. S1**). As a result, dFe concentrations were tightly coupled to L_1 ligands in an ~1:1 ratio (dFe: L_1, **Fig. 1d**) similar to previous studies in other neutrally buoyant plumes (**Fig. 1e**)[2,12,18]. However, the strong coupling between dFe and ligands was only observed at sites where L_1 ligands were detected. Some sampling locations contained high concentrations of weaker ligands (log $K^{cond}_{Fe',FeL}$ < 12, **Supplementary Table 2**) with no correlation to dFe. The weak ligands were either not saturated with Fe, or contained extremely high concentrations of dFe (> 20 nM) indicating potential sampling of a rising buoyant plume.

Altogether, our results suggest that L_1 ligands uniquely set the dFe concentration in these neutrally-buoyant plumes. A similar direct control of dFe concentrations by L_1 ligands has been previously observed in rivers[7] and aerosol solubility experiments[19]. Both the dFe and L_1 ligands could originate from the high temperature vents themselves, yielding a tightly coupled hydrothermal endmember. However, the concentration of L_1 ligands did not correlate with excess mantle Helium-3 ($^3He_{xs}$, **Fig S2**, **Supplementary Table 2**)[18], a nearly conservative tracer of the mixing of hydrothermal fluids with seawater[2]. These results suggest that L_1 ligands along the MAR are likely not sourced from the vent fluids themselves. All known sources of L_1 ligands ultimately have a biological origin, and the L_1 ligands observed here could be sourced from either entrainment of surrounding seawater, production from vent-biota and/or microbial mats, diffusion from sediments, or *in-situ* production by microbes within the neutrally buoyant plume[20].

Microbial organic ligand production has been suggested to tightly control the global oceanic trace metal inventories in both hydrothermal plumes[21,22] and the open ocean[11]. To explore this tight coupling between Fe and microbially-mediated ligand production within hydrothermal plumes, we used a novel state-of-the-art liquid chromatography coupled to electrospray ionization mass spectroscopy[23] method to screen our samples against a custom library of 500

known siderophores. Siderophores have Fe-binding constants that would operationally define them as L_1 ligands[4,9]. While potentially important in hydrothermal plumes, they have never been directly measured[14]. From our targeted approach, we identified that at least 0.01-0.66% of the L_1 ligands were microbially produced siderophores with high confidence (**Table 1**).

The siderophores we measured were found in picomolar concentrations, similar to other upper ocean marine environments[3,4,23,24]. Our estimate is a very conservative lower bound on siderophore concentrations due to (1) reporting only siderophores that we have identified with high confidence (40% of the total identifications across all samples, **Fig 2a**, **S3**), (2) detection limits based on small sample volumes, and (3) the 60-80% extraction efficiency for total dissolved organic matter[25] of our solid phase extraction technique. It is likely that known siderophores only represent a small fraction of the total siderophores expected to be produced in nature[26] and we are likely missing many unknown compounds. Yet, based on these results, the presence of microbially produced siderophores is evident and suggests several surprising aspects of Fe cycling in hydrothermal plumes. The biosynthesis of a siderophore is energy-intensive and is regulated by Fe concentration in the surrounding environment. Thus, the presence of siderophores suggests that bacteria are producing these compounds despite the overall higher Fe concentrations in the deep sea, and siderophore production is needed to transform Fe from these otherwise inaccessible forms. Finally, the direct detection of siderophores in these samples provides evidence that microbial ligand production is responsible for some portion of the tight coupling between strong ligands and dFe in hydrothermal systems along the MAR.

Chemical composition of siderophores in hydrothermal systems

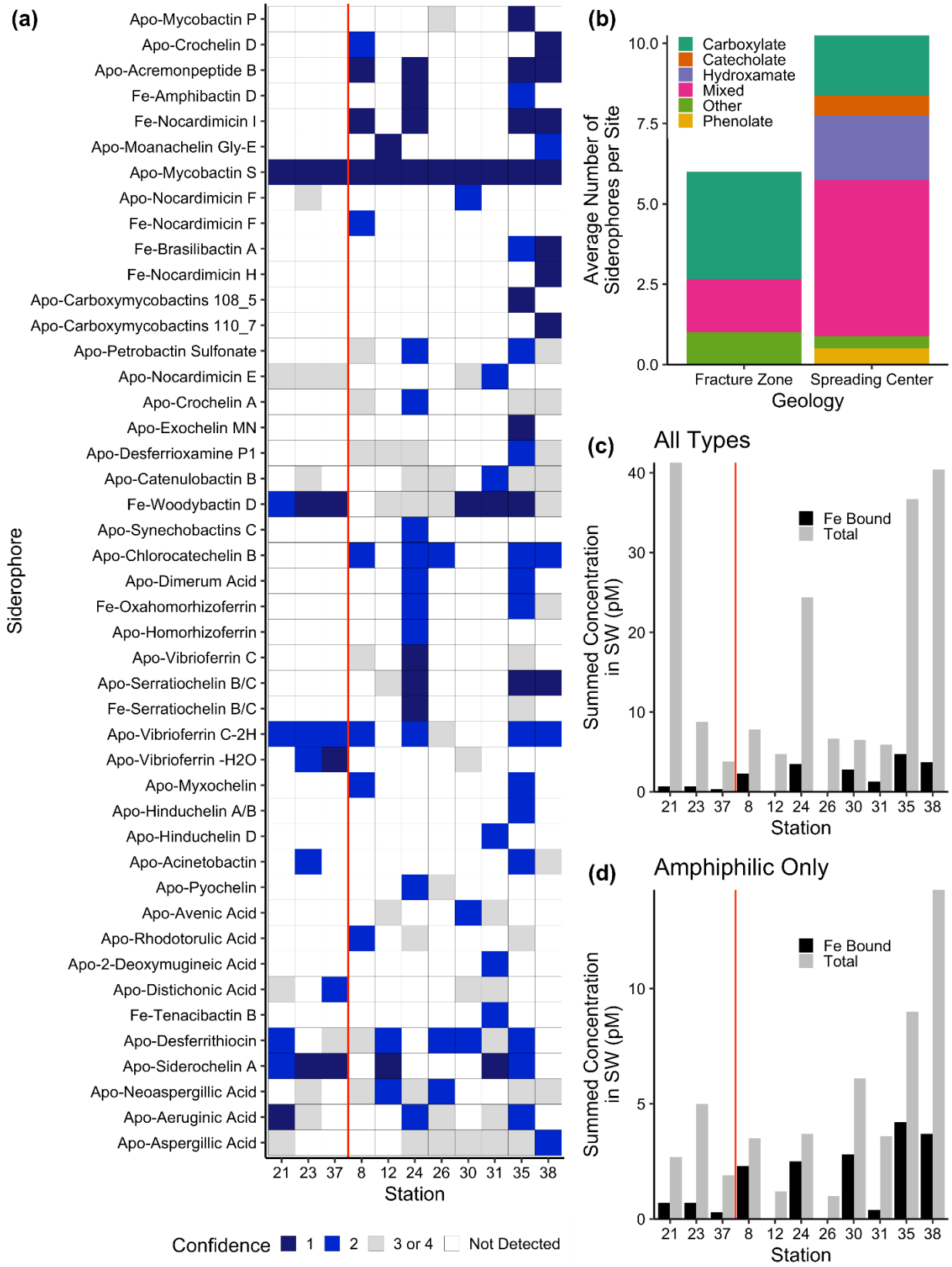

Figure 2. Siderophore presence in hydrothermal plumes along the MAR. (a) Heat map of confidence levels 1-2 (blue gradient, 1 = highest confidence). White boxes indicate siderophores that were either not detected or detected with lower confidence at those sites. The y-axis is ordered from top to bottom in terms of descending mass of the apo-form (without Fe) of the siderophore. (b) Bar graph of the types of siderophores identified with confidence levels of 1 and 2. Fe bound versus total summed concentration of (c) all types of siderophores and (d) amphiphilic siderophores at each station. The vertical red lines separate samples from fracture/diffuse sites on the left and samples from spreading centers on the right as defined in **Table 1**.

Marine ligand composition has been shown to change with environmental gradients[23], making the structure and functional groups of siderophores identified in and around hydrothermal samples of particular interest. Samples collected from on-axis spreading centers contained the highest dFe concentrations (> 20 nM) and samples from fracture zones, diffuse and off-axis sites contained the lowest dFe (≤ 1 nM). Spreading centers contained a wider variety of siderophore types than diffuse/fracture zones, with the greatest number of distinct siderophore compounds identified at the Broken Spur, Rainbow, and TAG vent sites (**Fig. 2**). On average, 10 compounds were identified with high confidence per spreading center sample, compared with only 6 identifications per diffuse/fracture zone sample (**Fig. 2b, Fig. S4-5**). Mixed-type siderophores — siderophores containing multiple moieties that bind to Fe(III) — were most common at or around spreading centers, while carboxylate-type siderophores — siderophores with both carboxyl and hydroxyl groups — were the most common at diffuse/fracture zones. Hydroxamates, phenolates, and catecholates were all identified at and around spreading centers, yet none of these types were detected in samples from diffuse/fracture zones. At spreading centers, neutrally buoyant plumes at on-axis vents averaged twice the number of distinct siderophore types than off-axis sites (**Fig. S6**), suggesting the proximity to the vent field plays an important role in the diversity and abundance of siderophore types produced by the microbial community.

Low Fe surface waters have been found to contain higher concentrations of amphiphilic siderophores compared to high Fe waters[23]. Amphiphilic siderophores have long hydrocarbon tails that can be embedded into the lipid bilayer of the bacterial cell membrane providing a mechanism to shuttle Fe into the cell and preventing diffusive loss of Fe[27]. As a result, these microbes have a competitive advantage over other bacteria that produce non-amphiphilic siderophores which more easily disperse away from the cell in solution. Amphiphilic siderophores accounted for over a third (38%) of the high confidence siderophores observed in our samples (**Fig. S7**). These siderophores also tended to have higher molecular weights than

those detected with lower confidence (**Fig. S8**). This either suggests our current methods for identifying siderophores in environmental samples may select for higher molecular weight compounds, or that amphiphilic siderophores are very common in marine environments[28]. It is surprising that they were so common in our dataset, due to the elevated Fe concentrations observed here relative to more Fe-poor surface ocean. Amphiphilic siderophores were found in total concentrations between 1.0-18.9 pM, with Rainbow and TAG containing the highest concentrations (8.9±0.76 and 18.9±1.4 pM respectively; **Fig. 2d**, **Supplementary Table 4**). Interestingly, these concentrations were similar or higher than previously observed in other upper ocean marine environments[3,23,29]. Marine bacteria have been shown to produce suites of amphiphilic siderophores as a way to adapt to the change in hydrophilicity in the surrounding environment[30,31], which could be an important coping strategy for bacteria living in environments with strong chemical gradients enabling them to access the varying forms of Fe. Unlike in the surface ocean where high concentrations of amphiphilic siderophores are observed in regions where Fe is a growth-limiting micronutrient[23], amphiphilic siderophore production in hydrothermal plumes could be a way for bacteria store Fe as they are physically transported in and away from the plume. This could be similar to how the production of multiple siderophores in terrestrial and pathogenetic systems are used to uptake inorganic Fe for cellular uptake, Fe storage, and absorption of other metals in association with Fe[26].

Microbial sources of siderophores in hydrothermal plumes

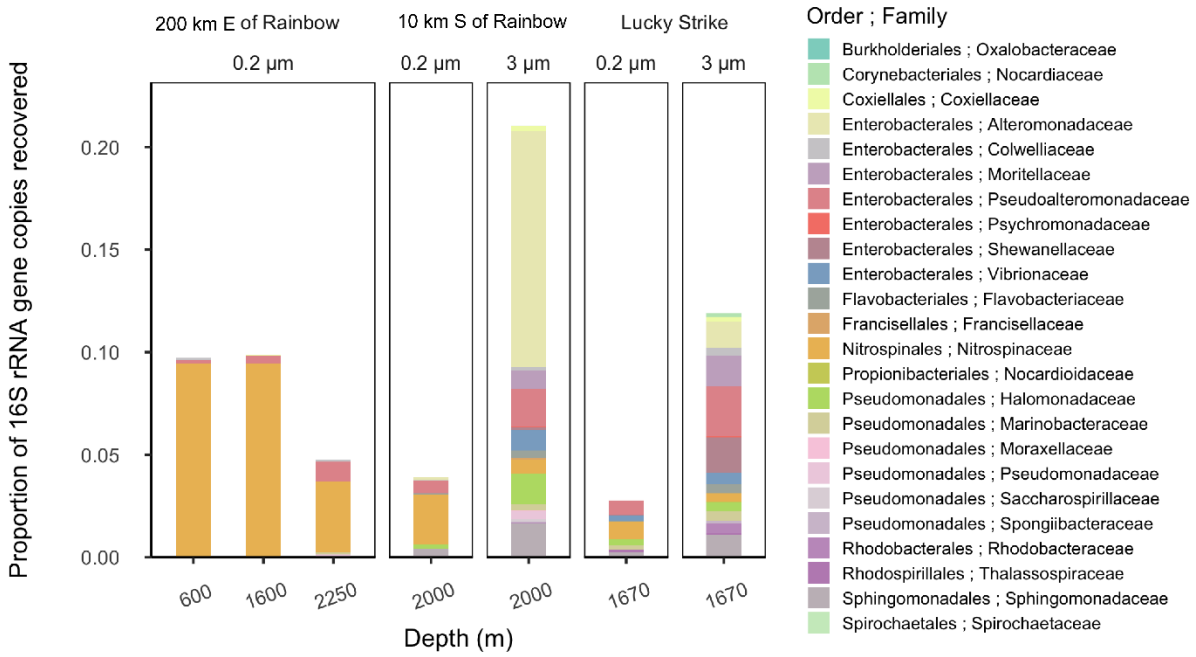

Figure 3. Relative abundance of putative siderophore-producing taxa. Bar height indicates the proportion of 16S rRNA genes recovered in each sample, separated by depth, filter size fraction, and site location. Colors correspond to taxonomy. Genera found in MAR vent microbial communities with members in the antismash database predicted to produce siderophores are depicted at the family level.

Microbial production of siderophores is a strategy for organisms to adapt or compete with other bacteria for Fe within a specific environment[30] and points to a coupling of organic ligand production and dFe concentrations. We examined the microbial community composition around Rainbow (St. 11- 200 km E of Rainbow and St. 17- 10 km S of Rainbow) and Lucky Strike (St. 7; **Table 1, Supplementary Table 1**) using 16S rRNA gene-based amplicon sequencing to determine the presence of microbes that may have the metabolic potential to synthesize the siderophores we observed at Rainbow, 30 km E of Rainbow and Lucky Strike (**Fig. 3, S9**). Diagnosing metabolic function from 16S rRNA data alone is limited, however exploring whether taxa present in these vent sites are encoding siderophore biosynthetic gene clusters indicates whether the microbial community is genetically capable of producing the compounds we observed in the environment. Bacterial genera containing known siderophore-producers were found at all three MAR sites examined, and putative siderophore-producers represented 3-20% of the relative abundance of each community (**Fig. 3**). Putative siderophore-producers were more

abundant in the 3 µm (particle-attached) size fraction than in the 0.2 µm (free-living) fraction, suggesting siderophore production is more common in particle-associated bacteria in hydrothermal environments.

We found microbial genera in our samples that have previously been shown to produce a subset of the siderophores identified here, including ferrioxamines, vibrioferrin, and acinetoferrin[3,4,8,10,23]. Genera with the genetic potential to produce ferrioxamines were present at all three sites, while those known to produce vibrioferrin were present at Lucky Strike and 10 km S of Rainbow and those producing acinetoferrin present at 10 km S of Rainbow (**Supplemental Table 1, 5**). Mycobactins were detected with high confidence in every sample of this study and were isolated from a cultured organism from a hydrothermal system[32], but no putative mycobactin producers were identified in the 16S rRNA data in this study. We also detected woodybactin D with high confidence in six out of our eleven sites. Although these biosynthetic genes were not identified in any of the genera from our 16S rRNA gene amplicon sequences, woodybactin D is a carboxylate siderophore isolated from *Shewanella*[33], and groups of deep-sea *Shewanella*[34] were found in the 16S rRNA data (**Fig. S9**). The biosynthesis genes for many of the siderophores we identified are unknown, and thus the fact that we only found genera capable of producing a subset of the siderophores we characterized in the water column is not surprising. However, the observation that a significant portion of the *in-situ* microbial community is capable of synthesizing siderophores (**Fig 3**) suggests that siderophore production is more widespread in the marine environment and in the deep ocean than previously believed.

Although the production of siderophores is often assumed to be associated primarily with low Fe conditions, evidence that siderophores are ubiquitous in marine environments, including those relatively rich in Fe, has been increasing. These regions are relatively high in Fe in comparison to the open ocean, but are depleted relative to terrestrial environments and requirements for bacteria growth[35]. Thus, the higher dFe associated with hydrothermal plumes may still not be high enough to suppress siderophore production. It is also likely that in higher Fe environments, such as hydrothermal plumes, not all of the Fe is bio-accessible. For example, soil microbes actively secrete siderophores in the high Fe soil environment to solubilize otherwise inaccessible particulate Fe[36]. Similar processes could be occurring in hydrothermal plumes, where Fe mineral

phases are common[37]. It is telling that most siderophore-producing genera were found in the particulate size fraction (**Fig. 3**), providing additional evidence that siderophores might be produced to solubilize different forms of particulate Fe. Further work that assesses why bacteria are producing siderophores in high Fe neutrally buoyant plumes will be important for understanding the role of these complexes in facilitating the exchange of Fe between dissolved and particulate phases[38], and how Fe-siderophore complexes may be stabilizing dFe in hydrothermal plumes.

Organic Fe-binding ligands have been implicated in playing a critical role in the preservation and transport of hydrothermal Fe into the ocean interior[2,17,38–43]. In this work, we have identified L_1 ligands as being tightly coupled to dFe in neutrally buoyant hydrothermal plumes along the MAR, and have provided evidence that these ligands are biologically produced. We identified specific siderophores that demonstrate a lower bound on the concentrations of L_1 ligands being produced by the microbial community in response to external Fe inputs. Bacteria putatively capable of synthesizing the siderophores were largely present in the particulate size fraction along the MAR, which adds to a growing body of evidence that microbes are likely using L_1 ligands to access particulate or otherwise inaccessible Fe pools and siderophores are a key mechanism for controlling dFe in neutrally buoyant plumes. Understanding whether tightly coupled Fe inputs and organic ligand production is present across all hydrothermal vent systems will aid in constraining the biogeochemical importance of microbial feedbacks in impacting the hydrothermal dFe supply to the deep ocean.

Methods

Sampling and cruise transect

Samples were collected as part of the 2017-2018 U.K. GEOTRACES GA13 section cruise along the Mid-Atlantic Ridge. Water samples from 11 venting and near venting locations were collected using a Seabird 911 conductivity, temperature, and depth (CTD) titanium rosette using conducting Kevlar wire with an oxidation-reduction potential (ORP) sensor to detect plumes. Teflon coated OTE (Ocean Test Equipment) bottles were pressurized to approximately 7 psi

with 0.2 µm filtered air using an oil free compressor. A Sartobran 300 (Sartorius) filter capsule (0.2 µm) was used to collect filtered seawater samples into clean 250 mL LDPE sample bottles. Bottles and caps were rinsed 3 times with the filtered sample before being filled. Samples were stored frozen at -20˚C for Fe-organic ligand characterization by voltammetry and mass spectrometry.

Fe-binding ligand concentrations and binding strengths

Competitive Ligand Exchange-Adsorptive Cathodic Stripping Voltammetry

Fe-binding ligand concentrations and binding strengths were determined by competitive ligand exchange-adsorptive cathodic stripping voltammetry (CLE-ACSV) with a BAS*i* controlled growth mercury electrode (CGME) with an Ag/$AgCl^-$ reference electrode and platinum auxiliary electrode (Bioanalytical Systems Incorporated). Using previously established methods[2,3,12,44,45], 40 frozen filtrate (<0.2 µm) samples with dFe concentrations between 0.41- 11.67 nM (**Supplementary Table 1-2**) were thawed in a 4˚C fridge prior to analysis. A 15-point titration curve was analyzed for each sample. Briefly, within each titration, every point sequentially received 10 mL of sample, 7.5 µM of borate-ammonium buffer, 10 µM salicylaldoxime (SA) added ligand, and a dFe addition. Data was collected using the *Epsilon Eclipse Electrochemical Analyzer* (v.213) with a deposition time of 120 seconds and analyzed using *ElectroChemical Data Software* (v2001-2014) and *ProMCC* (v2008-2018) to determine peak areas and Fe-binding ligand parameters, respectively.

Reverse Titration-CLE-ACSV

Reverse titration-CLE-ACSV (RT-CLE-ACSV)[46] was completed on 10 samples from Broken Spur, and TAG hydrothermal vent fields with dFe concentrations between 19.01-90.25 nM (**Supplementary Table 1-2**). Briefly, a 10-point titration curve was analyzed for each sample with each titration point consisting of 10 mL of sample buffered with 7.5 µM boric acid and the competitive ligand 1-nitroso-2-napthol (NN) additions. All samples were analyzed on a BAS*i* Controlled Growth Mercury Electrode (CGME) with the *Epsilon Eclipse Electrochemical Analyzer* (v.213) and deposition time of 120 seconds. For each sample, competitive ligand NN additions were 0.5, 1, 2, 3, 4, 6, 9, 15, 20, and 40 µM. Samples were equilibrated overnight and purged with N_2 (99.99%) for 5 minutes before analysis. At the end of each titration, three Fe

additions (3-15 nM) were added to the final titration point to get the total concentration of Fe in equilibrium with ligands. Data was analyzed using *ElectroChemical Data Software* (v2001-2014) to acquire peak areas and a package in R using the model parameters of β_{FeNN3} = 5.12 x 10^{16}, χ_{min} = 0.8, χ_{max} = 0.9, and *c1high* = 0.75 to determine the Fe-binding ligand parameters[46]. These parameters were chosen based on the recommendations for undersaturated samples and titrations curves where ip_{max} was not reached[46]. All other parameters within the model we kept at the default values.

Fe-binding organic ligand quantification and characterization

In addition to determining the total concentrations of strong Fe-binding ligands (L_1), we also identified and quantified siderophores that contributed to the L_1 ligand pool. Between 0.65-1.5 L of 0.2 µm filtered seawater sample (described above) was pumped slowly (15-20 mL min^{-1}) onto a polystyrene-divinylbenzene (Bond Elut ENV) solid phase extraction (SPE) column[3,23]. SPE columns were rinsed with MilliQ and stored at -20ºC until analysis. For the analytical measurements, samples were thawed in the dark, eluted in 12 mL of distilled methanol, and dried down to between 0.2-0.5 mL (**Supplementary Table 1**). Sample aliquots were analyzed by reverse-phase liquid chromatography (LC) on a trace metal clean bio-inert LC (Thermo Dionex 3000 NCS). The LC was interfaced with an electrospray ionization-mass spectrometer (ESI-MS; Thermo Q-Exactive HF) to identify and quantify the compounds based on exact mass (MS^1) and the fragmentation (MS^2) data[3,23]. A 4-point standard curve with known concentrations of ferrioxamine E was used to quantify the identified siderophores. MS^1 peak areas were determined for all identified siderophores and peak areas were converted to concentration using the peak areas from the desferrioxamine E standard curve (**Fig. S14**). Commercial standards are not available for all of the siderophores identified, and different compounds have distinct ionization efficiencies in ESI-MS. Thus, the siderophore concentrations reported here are estimates of siderophore concentrations in these environments. Additionally, 1 mM of cyanocobalamin was added as an internal standard to each sample aliquot to address any changes in sensitivity during LC-MS runs.

MSconvert (Proteowizard) was used to convert ESI-MS data to an open source mzxML format, and two stages of data processing were conducted using modified versions of previously reported

R scripts[3,23]. In the first stage, mzxML files were read into R using new package "RaMS" (https://github.com/wkumler/RaMS) which eased analysis, searched for masses of interest from an in-house database of siderophores in MS^1 data, and identified candidates based on a series of filters. The masses of interest were the ionized apo, ^{54}Fe-bound, and ^{56}Fe-bound version of each siderophore, with a tolerance of 7.5 ppm. MS^1 spectra were quality controlled to contain a minimum of 25 datapoints or maximum intensity of each mass of interest greater than 1000 counts. Spectra meeting these criteria and containing either ^{54}Fe-bound and ^{56}Fe-bound peaks within 30 seconds of each other or peak for the apo form of interest were displayed for the user to make the final decision of whether to move on to stage two of processing with a given siderophore.

Stage two of processing compared MS^2 spectra of the apo and Fe-bound forms of candidate siderophores with the predicted MS^2 generated by *in silico* fragmenter MetFrag[47]. The *in silico* fragmenter feature was run with a tolerance of 10 ppm on "$[M+H]^+$" and "$[M+Na]^+$" modes. A confidence level of 1-4, from highest to lowest confidence, was then assigned to candidates based on the following criteria: (1) peaks were present in MS^1 and MS^2 spectra, and, and at least one of the three most-intense peaks match *in silico* fragmentation, (2) peaks were present in MS^1 and MS^2 spectra, and small-intensity peaks in the MS^2 match *in silico* fragmentation, (3) peaks were present in MS^1 and MS^2 spectra, but little to no fragments in the MS^2 match *in silico* fragmentation, and (4) good peaks were identified in MS^1 spectra but not in MS^2 spectra (**Fig. S10-13)**. MetFrag pulls chemical structures from publicly-available databases like PubChem or COCONUT[48], which contain most, but not all variations of siderophores. As such, Fe-bound candidates were usually run against the apo form available in the database, and for siderophores with similar structures but variations in fatty chain length or double bond placement, sometimes only one parent structure was available.

Microbial community analysis

Microbial community composition was assessed in neutrally buoyant plumes and near venting sites at three sites: Lucky Strike (Station 7; 1670 m), 10 km S of Rainbow (Station 17; 2000 m), and 200 km E of Rainbow (Station 11; 600 m, 1600 m and 2250 m). One to 2 L of seawater were filtered by pressure filtration through sequential 25 mm membrane filters housed in

polypropylene filter holders (Whatman SwinLok, GE Healthcare, Pittsburgh, Pennsylvania) using a peristaltic pump and silicone tubing. Samples first passed through a 3 µm pore-size polyester membrane filter (Sterlitech, Auburn, Washington) then onto a 0.2 µm pore-size polyethersulfone membrane filter (Supor-200, Pall Corporation, Port Washington, New York). Pump tubing was acid washed with 10% hydrochloric acid and flushed with ultrapure water between each sample. The filters were flash frozen in liquid nitrogen in 2 mL gasketed bead beating tubes (Fisher Scientific) at sea.

Nucleic acids (DNA) were extracted as described previously[49], with slight modifications. Briefly, cells on the filters were lysed directly in the bead beating tubes with sucrose-ethylene diamine tetraacetic acid (EDTA) lysis buffer (0.75 M sucrose, 20 mM EDTA, 400 mM NaCl, 50 mM Tris) and 1% sodium dodecyl sulfate. Tubes were then agitated in a bead beating machine (Biospec Products) for 1 min, and subsequently heated for 2 min. at 99°C in a heat block. Proteinase K (New England Biolabs) was added to a final concentration of 0.5 mg/mL. Filters were incubated at 55°C for approximately 4 h and the resulting lysates were purified with the DNeasy kit (Qiagen) using a slightly modified protocol[49]. The purified nucleic acids were eluted in 200 µL of DNase, RNase-free water, and quantified using a fluorometer (Qubit and Quanti-T HS reagent, Invitrogen Molecular Probes).

The 16S rRNA gene was amplified in all samples using V4 primers[50,51] (515F-Y and 806RB) following a previously established protocol[52]. Amplicons were sequenced using a paired-end 250bp run on an Illumina MiSeq 500 and demultiplexed by the UC Davis Genome Center. The resulting 16S rRNA amplicon sequences were filtered and trimmed using the DADA2 pipeline in R[53]. Taxonomic assignments were made with version 138.1 of the SILVA SSU database[54] (silva_nr99_v138.1_wSpecies_train_set.fa.gz ; doi:10.5281/zenodo.4587955; accessed March 2022). Chloroplast and mitochondrial sequences were filtered out of the dataset using the 'phyloseq' R package (v 1.38.0), after which samples had read depths ranging from 9375 – 65486 reads (average 28425 $\pm$ 20014 reads) and represented 1010 unique amplicon sequence variants (ASVs). Read counts were transformed from absolute to relative abundance and taxa were aggregated to the Family level. The ten most abundant families present in each sample were visualized using the 'ggplot2' package (v. 3.3.5).

In order to assess the potential of the observed prokaryotic taxa to produce siderophores, we downloaded all siderophore biosynthetic gene clusters (BGCs) in the antismash secondary metabolite database (*n* = 7909) and used text-string matching to compare genera containing these BGCs to the genera found in our 16S rRNA gene dataset[55]. We cross-referenced the nomenclature of antismash-predicted siderophores with that of the siderophores identified by LC-ESI-MS in this study, accounting for minor differences in naming convention between the two databases, to determine if microbial community members present at each site were predicted to make any of the siderophores that were measured at that site. Station 38 and Station 12 were the closest sites with siderophore measurements for comparison against the taxonomic samples taken at 200 km E of Rainbow and 10 km S of Rainbow, respectively. Samples for microbial taxonomy and siderophore identity were taken from the same location at Lucky Strike and thus directly compared.

Data Availability

The CSV data reported in this study has been deposited at Zenodo under the DOI: http://doi.org/10.5281/zenodo.7325154. The LC-ES-MS data has been deposited on Massive under the DOI: http://doi.org/doi.10.25345/C5V97ZW7N. Microbial 16S rRNA data have been deposited on GenBank under the accession number BioProject #PRJNA865382. All data is freely available on each of these data repositories.

Acknowledgments

We acknowledge the captain and crew of the R/V *James Cook*, Chief Scientist Alessandro Tagliabue, and Noah Gluschankoff for supporting this work. This study was a part of the FeRidge project (GEOTRACES section GA13) which was supported by the Natural Environment Research Council funding (NERC United Kingdom Grants NE/N010396/1 to MCL and NE/N009525/1 to AT). The International GEOTRACES Programme is possible in part thanks to the support from the U.S. National Science Foundation (Grant OCE-1840868) to the Scientific Committee on Oceanic Research (SCOR). CLH was funded by JISAO/CICOES postdoctoral fellowship. PJM was funded through the NOAA Hollings Scholar summer program.

JR was funded by NOAA Ocean Exploration and Research, NOAA Earth-Ocean Interactions programs at NOAA-Pacific Marine Environmental Labs, and JISAO/CICOES. Part of this work was carried out in the University of Washington TraceLab, which receives support from the M.J. Murdock Charitable Trust in conjunction with the University of Washington College of Environment, and the Pacific Marine Environmental Labs at the National Oceanic and Atmospheric Administration. Parts of this work was also carried out in Dr. Anitra Ingalls laboratory with the help of Laura Truxal and Dr. Jiwoon Park at the University of Washington-School of Oceanography.

Author Contributions

Manuscript preparation, sample/data processing, CSV analysis, and interpretation (C.L.H.), manuscript preparation, LC-ESI-MS data analysis and interpretation (P.J.M.), microbial analysis and interpretation (J.B.A. and A.E.S.), dissolved iron and derived excess $^{3}He_{xs}$ measurements, sample collection (A.J.M. L. and M.C.L.), microbial data collection and ligand data interpretation (T.M. and K.N.B.), and project design and planning, data interpretation, and mentoring (A.T., M.C.L., J.A.R., and R.M.B.). All authors were involved in editing manuscript.

Competing Interests

The authors declare no competing interests.

References

1. Tagliabue, A. *et al.* The integral role of iron in ocean biogeochemistry. *Nature* **543**, 51–59 (2017).

2. Buck, K. N., Sedwick, P. N., Sohst, B. & Carlson, C. A. Organic complexation of iron in the eastern tropical South Pacific: Results from US GEOTRACES Eastern Pacific Zonal Transect (GEOTRACES cruise GP16). *Mar. Chem.* **201**, 229–241 (2018).

3. Bundy, R. M. *et al.* Distinct Siderophores Contribute to Iron Cycling in the Mesopelagic at Station ALOHA. *Front. Mar. Sci.* 1–15 (2018). doi:10.3389/fmars.2018.00061

4. Moore, L. E., Heller, M. I., Barbeau, K. A., Moffett, J. W. & Bundy, R. M. Organic complexation of iron by strong ligands and siderophores in the eastern tropical North Pacific oxygen deficient zone. *Mar. Chem.* **236**, 104021 (2021).

5. Fishwick, M. P. *et al.* Global Biogeochemical Cycles on the dissolution of aerosol iron.

Global Biogeochem. Cycles **28**, 1235–1250 (2014).

6. Bundy, R. M. *et al.* Iron-binding ligands and humic substances in the San Francisco Bay estuary and estuarine-influenced shelf regions of coastal California. *Mar. Chem.* **173**, 183–194 (2015).

7. Buck, K. N., Lohan, M. C., Berger, C. J. M. & Bruland, K. W. Dissolved iron speciation in two distinct river plumes and an estuary: Implications for riverine iron supply. *Limnol. Oceanogr.* **52**, 843–855 (2007).

8. Butler, A. Marine siderophores and microbial iron mobilization. *Biometals* **18**, 369–374 (2005).

9. Manck, L. E. *et al.* Petrobactin, a siderophore produced by Alteromonas, mediates community iron acquisition in the global ocean. *ISME J.* **16**, 358–369 (2022).

10. Vraspir, J. M. & Butler, A. Chemistry of marine ligands and siderophores. *Ann. Rev. Mar. Sci.* **1**, 43–63 (2009).

11. Lauderdale, J. M., Braakman, R., Forget, G., Dutkiewicz, S. & Follows, M. J. Microbial feedbacks optimize ocean iron availability. *Proc. Natl. Acad. Sci. U. S. A.* **117**, 4842–4849 (2020).

12. Buck, K. N., Sohst, B. & Sedwick, P. N. The organic complexation of dissolved iron along the U.S. GEOTRACES (GA03) North Atlantic Section. *Deep. Res. Part II Top. Stud. Oceanogr.* **116**, 152–165 (2015).

13. Kleint, C., Hawkes, J. A., Sander, S. G. & Koschinsky, A. Voltammetric Investigation of Hydrothermal Iron Speciation. *Front. Mar. Sci.* **3**, 1–11 (2016).

14. Li, M. *et al.* Microbial iron uptake as a mechanism for dispersing iron from deep-sea hydrothermal vents. *Nat. Commun.* **5**, 3192 (2014).

15. Beaulieu, S. E. & Szafrański, K. M. InterRidge Global Database of Active Submarine Hydrothermal Vent Fields Version 3.4. (2020). doi:10.1594/PANGAEA.917894

16. Omanović, D., Garnier, C. & Pižeta, I. ProMCC: An all-in-one tool for trace metal complexation studies. *Mar. Chem.* **173**, 25–39 (2015).

17. Resing, J. a. *et al.* Basin-scale transport of hydrothermal dissolved metals across the South Pacific Ocean. *Nature* **523**, 200–203 (2015).

18. Lough, A. J. M. *et al.* The impact of hydrothermal vent geochemistry on the addition of iron to the deep ocean. *Biogeosciences Discuss.* **[preprint]**, 1–23 (2022).

19. Fishwick, M. P. *et al.* The impact of changing surface ocean conditions on the dissolution of aerosol iron. *Global Biogeochem. Cycles* **28**, 1235–1250 (2014).

20. Mellett, T. *et al.* Particle exchange mediated by organic ligands in incubation experiments of hydrothermal vent plumes along the mid-Atlantic Ridge.

21. Cowen, J. P. & Bruland, K. W. Metal deposits associated with bacteria: implications for Fe and Mn marine biogeochemistry. *Deep Sea Res. Part A. Oceanogr. Res. Pap.* **32**, 253–

272 (1985).

22. Cowen, J. P., Massoth, G. J. & Feely, R. A. Scavenging rates of dissolved manganese in a hydrothermal vent plume. *Deep Sea Res. Part A. Oceanogr. Res. Pap.* **37**, 1619–1637 (1990).

23. Boiteau, R. M. *et al.* Siderophore-based microbial adaptations to iron scarcity across the eastern Pacific Ocean. *Proc. Natl. Acad. Sci.* **113**, 14237–14242 (2016).

24. Park, J. *et al.* Siderophore production and utilization by microbes in the North Pacific Ocean. *bioRxiv* 2022.02.26.482025 (2022). doi:10.1101/2022.02.26.482025

25. Waska, H., Koschinsky, A., Ruiz Chancho, M. J. & Dittmar, T. Investigating the potential of solid-phase extraction and Fourier-transform ion cyclotron resonance mass spectrometry (FT-ICR-MS) for the isolation and identification of dissolved metal-organic complexes from natural waters. *Mar. Chem.* **173**, 78–92 (2015).

26. Hider, R. C. & Kong, X. Chemistry and biology of siderophores. *Nat. Prod. Rep.* **27**, 637–657 (2010).

27. Martinez, J. S. *et al.* Structure and membrane affinity of a suite of amphiphilic siderophores produced by a marine bacterium. *Proc. Natl. Acad. Sci. U. S. A.* **100**, 3754–3759 (2003).

28. Butler, A. & Theisen, R. M. Iron(III)-siderophore coordination chemistry: Reactivity of marine siderophores. *Coord. Chem. Rev.* **254**, 288–296 (2010).

29. Boiteau, R. M. *et al.* Patterns of iron and siderophore distributions across the California Current System. *Limnol. Oceanogr.* **64**, 376–389 (2019).

30. Sandy, M. & Butler, A. Microbial iron acquisition: marine and terrestrial siderophores. *Chem. Rev.* **109**, 4580–95 (2009).

31. Homann, V. V *et al.* Loihichelins A - F , a Suite of Amphiphilic Siderophores Produced by the Marine Bacterium Halomonas LOB-5. *J. Nat. Prod.* **72**, 884–888 (2009).

32. Gu, H., Sun, Q., Luo, J., Zhang, J. & Sun, L. A First Study of the Virulence Potential of a Bacillus subtilis Isolate From Deep-Sea Hydrothermal Vent. *Front. Cell. Infect. Microbiol.* **9**, 1–14 (2019).

33. Carmichael, J. R., Zhou, H. & Butler, A. A suite of asymmetric citrate siderophores isolated from a marine Shewanella species. *J. Inorg. Biochem.* **198**, 1–6 (2019).

34. Kato, C. & Nogi, Y. Correlation between phylogenetic structure and function : examples from deep-sea Shewanella. **35**, 223–230 (2001).

35. Tortell, P. D., Maldonado, M. T. & Price, N. M. The role of heterotrophic bacteria in iron-limited ocean ecosystems. *Nature* **383**, 330–332 (1996).

36. Crowley, D. E., Wang, Y. C., Reid, C. P. P. & Szaniszlo, P. J. Mechanisms of iron acquisition from siderophores by microorganisms and plants. *Plant Soil* **130**, 179–198 (1991).

37. Hoffman, C. L. *et al.* Diagnostic morphology and solid-state chemical speciation of hydrothermally derived particulate Fe in a long-range dispersing plume. *ACS Earth Sp. Chem.* **4**, 1831–1842 (2020).

38. Fitzsimmons, J. N. *et al.* Iron persistence in the distal hydrothermal plume supported by dissolved – particulate exchange. *Nat. Geosci.* **10**, 1–8 (2017).

39. Hoffman, C. L. *et al.* Near-field iron and carbon chemistry of non-buoyant hydrothermal plume particles, Southern East Pacific Rise 15°S. *Mar. Chem.* **201**, 183–197 (2018).

40. Toner, B. M. *et al.* Preservation of iron(II) by carbon-rich matrices in a hydrothermal plume. *Nat. Geosci.* **2**, 197–201 (2009).

41. Bennett, S. a., Hansman, R. L., Sessions, A. L., Nakamura, K. ichi & Edwards, K. J. Tracing iron-fueled microbial carbon production within the hydrothermal plume at the Loihi seamount. *Geochim. Cosmochim. Acta* **75**, 5526–5539 (2011).

42. Bennett, S. a. *et al.* The distribution and stabilisation of dissolved Fe in deep-sea hydrothermal plumes. *Earth Planet. Sci. Lett.* **270**, 157–167 (2008).

43. Sander, S. G. & Koschinsky, A. Metal flux from hydrothermal vents increased by organic complexation. *Nat. Geosci.* **4**, 145–150 (2011).

44. Abualhaija, M. M. & van den Berg, C. M. G. G. Chemical speciation of iron in seawater using catalytic cathodic stripping voltammetry with ligand competition against salicylaldoxime. *Mar. Chem.* **164**, 60–74 (2014).

45. Hawkes, J. A., Connelly, D. P., Gledhill, M. & Achterberg, E. P. The stabilisation and transportation of dissolved iron from high temperature hydrothermal vent systems. *Earth Planet. Sci. Lett.* **375**, 280–290 (2013).

46. Hawkes, J. A., Gledhill, M., Connelly, D. P. & Achterberg, E. P. Characterisation of iron binding ligands in seawater by reverse titration. *Anal. Chim. Acta* **766**, 53–60 (2013).

47. Ruttkies, C., Schymanski, E. L., Wolf, S., Hollender, J. & Neumann, S. MetFrag relaunched: incorporating strategies beyond in silico fragmentation. *J. Cheminform.* **8**, 1–16 (2016).

48. Sorokina, M., Merseburger, P., Rajan, K., Yirik, M. A. & Steinbeck, C. COCONUT online: Collection of Open Natural Products database. *J. Cheminform.* **13**, 1–13 (2021).

49. Santoro, A. E., Casciotti, K. L. & Francis, C. A. Activity, abundance and diversity of nitrifying archaea and bacteria in the central California Current. *Environ. Microbiol.* **12**, 1989–2006 (2010).

50. Apprill, A., Mcnally, S., Parsons, R. & Weber, L. Minor revision to V4 region SSU rRNA 806R gene primer greatly increases detection of SAR11 bacterioplankton. *Aquat. Microb. Ecol.* **75**, 129–137 (2015).

51. Parada, A. E., Needham, D. M. & Fuhrman, J. A. Every base matters: Assessing small subunit rRNA primers for marine microbiomes with mock communities, time series and global field samples. *Environ. Microbiol.* **18**, 1403–1414 (2016).

52. Stephens, B. M. *et al.* Organic Matter Composition at Ocean Station Papa Affects Its Bioavailability, Bacterioplankton Growth Efficiency and the Responding Taxa. *Front. Mar. Sci.* **7**, (2020).

53. Callahan, B. J. *et al.* DADA2: High-resolution sample inference from Illumina amplicon data. *Nat. Methods* **13**, 581–583 (2016).

54. Quast, C. *et al.* The SILVA ribosomal RNA gene database project: Improved data processing and web-based tools. *Nucleic Acids Res.* **41**, 590–596 (2013).

55. Blin, K., Shaw, S., Kautsar, S. A., Medema, M. H. & Weber, T. The antiSMASH database version 3: Increased taxonomic coverage and new query features for modular enzymes. *Nucleic Acids Res.* **49**, D639–D643 (2021).

56. Bazylev, B. A. Allochemical Metamorphism of Mantle Peridoties in the Hayes Fracture Zone of the North Atlantic. *Petrology* **5**, 362–379 (1997).

57. Kelley, D. S. & Shank, T. M. Hydrothermal systems: A decade of discovery in slow spreading environments. *Geophys. Monogr. Ser.* **188**, 369–407 (2010).

Table 1. Characteristics of sample locations along the Mid Atlantic Ridge

Vent Names	Abbr.	Station	Geology	Host rock	Vent type	Spreading rate (mm/yr)	Siderophore concentration (pM)	Siderophore/L_1 ligand (%)*
Lucky Strike	LS	7/8	Spreading Center	gabbro	Black smoker	20.2	0.4-1.3	0.001±5.23
33 km E of Rainbow	CER	12	Spreading Center	-	-	-	0.5-2.4	0.02±0.27
Rainbow	R	38	Spreading Center	ultramafic	Black smoker	20.6	0.5-17.5	*n.a.*
Hayes Fracture Zone	HFZ	21	Fracture Zone	peridotites/gabbro	-	21.2	0.7-33.7	0.66±0.35
Lost City	LC	23	Fracture Zone	ultramafic/gabbro	Alkaline	22.6	0.4-3.7	0.12±0.08
Broken Spur	BS	24	Spreading Center	gabbro	Black smoker/diffuse	22.9	0.1-10.4	0.03±2.30
29 km N of TAG	CNT	26	Spreading Center	-	-	-	0.6-4.0	0.06±1.75
30 km W of TAG	CWT	30	Spreading Center	-	-	-	0.4-2.8	0.09±0.001
30 km E of TAG	CET	31	Spreading Center	-	-	-	0.3-1.2	0.11±0.0002
Trans-Atlantic Geotraverse	TAG	35	Spreading Center	gabbro	Black smoker	23.6	0.2-8.5	0.05±0.0004
Low Temp Slope	LTS	37	-	-	Diffuse fluids	-	0.3-1.6	0.06±0.03

Spreading rates along the Mid-Atlantic Ridge were gathered from the Interridge Database v3.4. Host rock groups were determined from previously discussed classifications[56,57]. Off-axis sites –33 km E of Rainbow, 29 km N of TAG, 30 km E of TAG, and 30 km W of TAG– were far-field locations of their respective vent field. Low Temp Slope was a diffuse-dominated site that was sampled for the first time as a part of this study.

Siderophore concentrations and the percent of L_1 ligand are reported for both confidence level 1 and 2. Average L_1 ligand and siderophore concentrations can be viewed in **Supplementary Table 3** and concentrations for individual siderophores can be observed in **Supplementary Table 4**.

*Standard deviations are reported to understand the spread of both the average siderophore and L_1 ligand data.
n.a.= unable to be determined
- = unknown

613